

# General-Purpose Retrieval-Enhanced Medical Prediction Model Using Near-Infinite History

**Junu Kim**

*Kim Jaechul Graduate School of AI  
KAIST  
Dajeon, Republic of Korea*

KJUNE0322@KAIST.AC.KR

**Chaeun Shim**

*Kim Jaechul Graduate School of AI  
KAIST  
Dajeon, Republic of Korea*

CHAEUN@KAIST.AC.KR

**Bosco Seong Kyu Yang**

*Department of Neurosurgery and Neurology  
Seoul National University Bundang Hospital  
Seongnam, Republic of Korea*

BOSCOSKYANG@OUTLOOK.COM

**Chami Im**

*Department of Surgery  
Seoul National University Bundang Hospital  
Seongnam, Republic of Korea*

CHAMI0921@GMAIL.COM

**Sung Yoon Lim**

*Department of Internal Medicine  
Seoul National University Bundang Hospital  
Seongnam, Republic of Korea*

NUCLEON727@GMAIL.COM

**Han-Gil Jeong\***

*Department of Neurosurgery and Neurology, Center for Artificial Intelligence in Healthcare  
Seoul National University Bundang Hospital  
Seongnam, Republic of Korea*

HAN.G.JEONG@GMAIL.COM

**Edward Choi\***

*Kim Jaechul Graduate School of AI  
KAIST  
Dajeon, Republic of Korea*

EDWARDCHOI@KAIST.AC.KR

## Abstract

Machine learning (ML) has recently shown promising results in medical predictions using electronic health records (EHRs). However, since ML models typically have a limited capability in terms of input sizes, selecting specific medical events from EHRs for use as input is necessary. This selection process, often relying on expert opinion, can cause bottlenecks in development. We propose Retrieval-Enhanced Medical prediction model (REMed) to address such challenges. REMed can essentially evaluate unlimited medical events, select the relevant ones, and make predictions. This allows for an unrestricted input size, eliminating the need for manual event selection. We verified these properties through experiments involving 27 clinical prediction tasks across four independent cohorts, where REMed outperformed the baselines. Notably, we found that the preferences of REMed align closely with those of medical experts. We expect our approach to significantly expedite the development of EHR prediction models by minimizing clinicians' need for manual involvement.

---

\*Co-corresponding author

## 1. Introduction

A patient’s medical records in a hospital are archived as a sequence of medical events (*e.g.*, lab measurements, prescriptions, procedures) in electronic health records (EHRs). In recent years, machine learning (ML) has shown remarkable potential in predicting various medical outcomes (*e.g.*, mortality, length of stay) using EHR data (Choi et al., 2016; Rajkomar et al., 2018; Wang et al., 2020). However, the sheer volume of events in EHRs presents a significant challenge for developing predictive models. For instance, a patient in an intensive care unit (ICU) typically generates thousands of events daily (Sanchez-Pinto et al., 2018). The computational requirements of ML models scale with the size of the input (Rumelhart et al., 1985; Vaswani et al., 2017), making it challenging to effectively harness all this information, even with efficient modern architectures specialized to handle long input (Choromanski et al., 2020; Gu et al., 2021; Ma et al., 2022).

Accordingly, heuristic event selection is required to reduce the input size. This process typically relies on human decisions made by domain experts, such as experienced clinicians, which is costly and time-consuming. This acts as a significant bottleneck in the model development process. While some recent studies have explored methods to alleviate the need for event selection, none have addressed the issue of limited input size, a fundamental reason for such selection (Rajkomar et al., 2018; Deasy et al., 2020; Steinberg et al., 2021; Nallabasannagari et al., 2020; Hur et al., 2023, 2022). As a result, none have completely eliminated the need for domain experts’ involvement. Therefore, our main objective is to develop a model capable of handling a near-infinite number of events, thereby eliminating this bottleneck.

Recent studies have explored methods to eliminate the need for feature selection (Rajkomar et al., 2018; Deasy et al., 2020; Steinberg et al., 2021; Nallabasannagari et al., 2020; Hur et al., 2023, 2022). Notably, empirical findings from some of these studies suggest that models incorporating more features often outperform those with selected features (Rajkomar et al., 2018; Nallabasannagari et al., 2020; Hur et al., 2022, 2023). In general, there are two dominant approaches to achieve this. Formally, a medical event  $e_i$  occurring at timestamp  $t_i$  is typically composed of a medical code  $c_i$  that provides high-level information (*e.g.*, a medical code “L123” denotes “Lab measure of white blood cells”), and accompanied details  $d_i$  (*e.g.*, “Value=3.7”, “Unit of Measurement=K/uL”, “Flag=abnormal”). The first way is mapping each  $c_i$  and  $d_i$  to a unique vocabulary (Rajkomar et al., 2018; Nallabasannagari et al., 2020; Deasy et al., 2020; Steinberg et al., 2021). However, given that a typical EHR contains tens of thousands of unique  $c_i$  and  $d_i$  (Johnson et al., 2016, 2020; Pollard et al., 2018), this method often struggles to handle the rare ones. The second approach treats both the  $c_i$  and  $d_i$  as text, mapping them to a natural language space (Hur et al., 2022, 2023). This method ensures that  $c_i$  and  $d_i$  with similar meanings (*e.g.*, the frequently occurred code “Non-invasive blood pressure systolic” and the less common “Manual blood pressure systolic”) are represented similarly, often outperforming the first approach (Hur et al., 2022, 2023). Among them, GenHPF (Hur et al., 2023) achieved superior performance by utilizing all information of  $d_i$ . However, none of these approaches have addressed the issue of limited input size, a fundamental reason for event selection. As a result, they all rely on manual observation window selection to limit the number of input events to a computationally feasible scale. This necessitates the involvement of domain experts, which

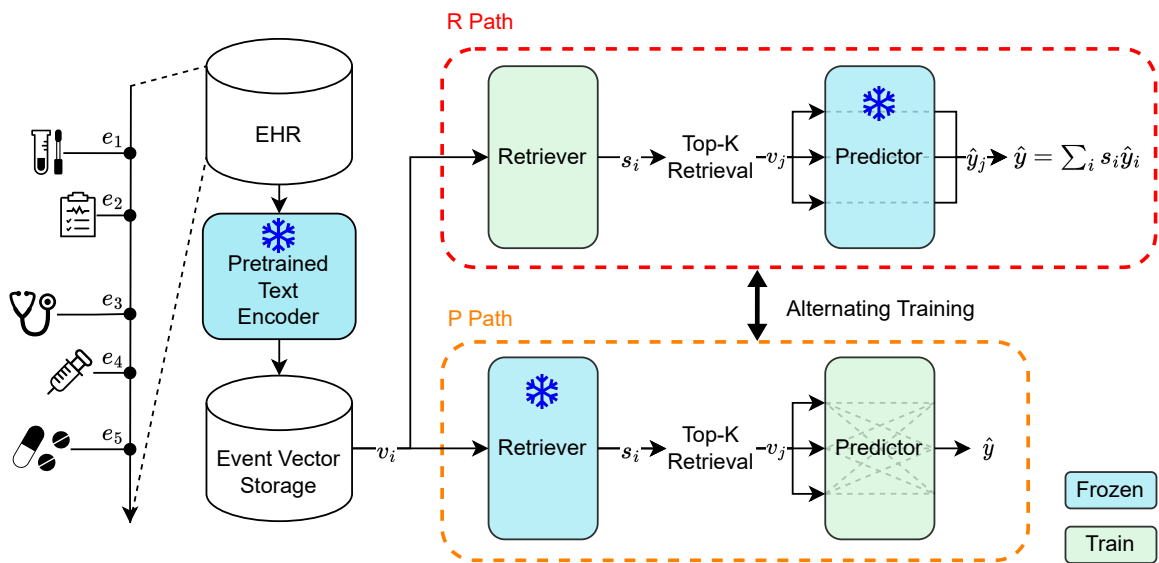


Figure 1: Model Architecture: REMed receives a series of event vectors as input, continuously identifies important events, retrieves them, and makes predictions. To ensure both Retriever and Predictor are trainable, our model alternates between two forward paths during the training stage. Note that the timestamps are omitted in this figure.

becomes a significant bottleneck in the model development process. Therefore, we aim to develop a model capable of handling a near-infinite number of events, thereby eliminating the need for feature and observation window selection.

We tackle this challenge by employing a Retrieval-Based Approach (RBA). RBA, which has been widely explored in the natural language processing (NLP) question-answering (QA) domain, operates in two primary steps: 1) retrieving a collection of documents relevant to a specific question and 2) using these documents to make informed predictions (Karpukhin et al., 2020; Lewis et al., 2020). Inspired by RBA’s capability to efficiently process millions of documents (Borgeaud et al., 2022), we adopt its methodology for managing virtually infinite medical events. Our model, named *Retrieval-Enhanced Medical prediction model* (REMed), 1) retrieves events that are useful for predicting the target outcome, and 2) performs a prediction by leveraging the correlations among these selected events (Figure 1). As a result, REMed can process a near-infinite number of events<sup>1</sup>, thereby eliminating the need for event selection, ultimately minimizing the domain expert involvement in the development process.

We trained REMed on 27 clinical prediction tasks, including mortality, length of stay, creatinine, and platelets prediction, using four independent cohorts from publicly available EHR datasets: MIMIC-IV (Johnson et al., 2020), eICU (Pollard et al., 2018), UMCdb (Pollard et al., 2018), and HIRID (Hyland et al., 2020). From this comprehensive evaluation, REMed showcased its superior performance compared to various baselines. Notably, REMed’s retrieval result is compatible with established medical knowledge.

<sup>1</sup>Further discussion about the near-infinite history is provided in Appendix A.5.

In this study, we utilized open-source datasets only and made all our codes accessible to the public, guaranteeing transparency and reproducibility of our results. In this study, we utilized open-source datasets only and made all our codes accessible to the public<sup>2</sup>, guaranteeing transparency and reproducibility of our results. We believe that REMed can accelerate the development of medical prediction models by minimizing the involvement of domain experts.

## Generalizable Insights about Machine Learning in the Context of Healthcare

A patient admitted to a hospital can generate millions of medical events in EHR, yet typical machine learning models possess limited capability in handling such extensive inputs. Therefore, selecting important medical events based on domain experts’ knowledge was essential to develop a medical predictive model. In this context, our contributions can be summarized as follows:

- We propose REMed, the first attempt to introduce the Retrieval-Based Approach to the medical prediction task using structured EHR data. REMed can handle virtually an unlimited number of events and demonstrates superior performance in handling a large number of events.
- REMed eliminates the fundamental need for event selection due to its ability to manage unlimited events. We empirically demonstrated that abstaining from such selection does not compromise the prediction performance.
- REMed can identify and retrieve clinically relevant events. We verified that the retrieval results are compatible with established clinical knowledge.

## 2. Backgrounds

### 2.1. Problem Definition

Formally, a patient’s medical history  $H$  can be represented as:

$$H = \{(e_1, t_1), (e_2, t_2), \dots, (e_i, t_i), \dots\}, \quad (1)$$

where  $e_i$  is the  $i^{th}$  medical event and  $t_i$  is its corresponding timestamp. Medical prediction aims to predict the specific outcomes of a patient (*e.g.*, mortality) at a certain time-point using the patient’s medical history, such that

$$\hat{y} = f(\{(e_i, t_i) | t_i < T\}), \quad (2)$$

where  $f$  is a prediction model, and  $T$  denotes the moment the prediction is carried out (*i.e.*, prediction time).

---

<sup>2</sup><https://github.com/starmppcc/REMed>

## 2.2. Event Selection

A medical event  $e_i$  occurring at timestamp  $t_i$  is typically composed of a medical code  $c_i$  and accompanied details  $d_i$ . There are two primary strategies in event selection: 1) Feature selection - This strategy focuses on selecting a particular set of  $c_i$ 's that are considered relevant to the prediction target; 2) Observation window selection - This strategy often selects recent events based on their  $t_i$ 's. However, since both strategies rely on the heuristic decision of domain experts, it acts as a bottleneck in the model development process.

## 2.3. Retrieval-Based Approach in Medical Domain

A typical application of RBA in the medical domain is the retrieval of appropriate clinical articles (Simpson et al., 2014; Roberts et al., 2015, 2016; Wei and Eickhoff, 2018). Furthermore, some research has aimed to enhance medical prediction performance by using retrieved documents related to a given patient’s diagnosis codes (Ye et al., 2021) or clinical notes (Naik et al., 2022). Additionally, another study has used RBA to retrieve clinical note snippets relevant to specific medical situations (Jiang et al., 2023). However, all these works have focused on retrieving clinical text. In contrast, our work aims to retrieve medical events from structured EHRs that are related to a given medical prediction task.

## 3. Retrieval-Enhanced Medical Prediction Model

This section explains our model architecture, as illustrated in Fig 1. While conventional approaches necessitate feature or observation window selection to reduce the number of events, we aim to build a model without such conditions. Consequently, as mentioned earlier, we start with GenHPF, which has demonstrated superior performance among the feature selection-free methods. Following this, we first convert each event  $e_i$  to its text representation  $r_i$  by first converting the code  $c_i$  to its description (e.g., “L123”  $\rightarrow$  “Lab measure for white blood cells”) and then concatenating with its accompanied details  $d_i$  (e.g., “Lab measure for white blood cells, Value 3.7, Unit of Measurement K/uL, Flag abnormal”).

Similar to the typical Retrieval-Based Approach (RBA) in question-answering (QA), each  $r_i$  is initially encoded into a dense vector  $v_i$  using a pre-trained text encoder  $Enc_{PT}$  (Alsentzer et al., 2019; Hur et al., 2023).

$$v_i = Enc_{PT}(r_i) \quad (3)$$

In a typical question-answering task, each document’s importance is calculated by comparing each document to the given query, which has theoretically an infinite degree of freedom (*i.e.*, a user can ask anything.). In contrast, for medical prediction tasks, typically a set of prediction targets (*e.g.*, mortality, readmission) is fixed<sup>3</sup>. As a result, evaluating the events with respect to queries that vary for each prediction is not required. Instead, we directly assess the scalar importance  $s_i$  of each event vector  $v_i$  while considering its timestamp  $t_i$  using Retriever  $R$ , which is implemented with a multi-layer perceptron (MLP),

$$s_i = R(v_i, t_i). \quad (4)$$

---

<sup>3</sup>One could try prompt-based medical prediction with a large language model (LLM), thus having unfixed prediction targets. Further discussion is provided in Appendix A.4.

In this way, the information related to the prediction targets is embedded in the parameters of  $R$ . Following this, the top- $k$  event vectors  $v_j$ , ranked by their scores  $s_j$ , are retrieved and fed into the Predictor  $P$  along with their respective timestamps  $t_j$ , which is implemented with Transformer (Vaswani et al., 2017).  $P$  interprets the meaning of events in relation to their surrounding events, making a prediction  $\hat{y}$ .

$$\hat{y} = P(\{v_j, t_j\}) \quad (5)$$

While processing all events simultaneously with a Transformer is impractical due to its high computational requirements, evaluating all events *independently* with an MLP is feasible. By limiting the input into the Transformer to only the most relevant events, we can harness the powerful predictive performance of the Transformer while also ensuring computational efficiency.

Our training objectives are twofold: To train  $R$  to understand the significance of each event, and to train  $P$  to exploit the correlations among events. It is, however, not straightforward to train  $R$  and  $P$  in an end-to-end manner, which requires that  $s_j$  directly affect  $\hat{y}$  while acting as an event importance indicator. Feeding  $s_j$  into equation 5 will only partially satisfy this requirement (see Appendix A.3 for further discussion on this point), and therefore we devise a new training strategy that involves two paths, namely the *R Path*, and the *P Path*. Each path exclusively trains one component,  $R$  or  $P$ , while keeping the other component frozen. Throughout the training process, we alternate between these two paths at each step. In the *R Path* (Figure 1, red box), we feed each event to the frozen  $P$  independently, making the same number of predictions as the number of retrieved events. These predictions are then combined based on their importance scores to make a final prediction.

$$\hat{y} = \sum_j s_j \hat{y}_j, \text{ where } \hat{y}_j = P(v_j, t_j) \quad (6)$$

Following this,  $s_j$  is directly affecting  $\hat{y}$  while acting as an event importance indicator, since  $R$  would be trained to increase  $s_j$  when  $\hat{y}_j$  is consistent with the label  $y$ . Therefore,  $R$  can learn to calculate the importance of each event. It might seem possible to train  $P$  using the *R Path*; however, this cannot train  $P$  effectively. Since each event is fed into  $P$  independently,  $P$  cannot learn the correlation between events using the *R Path* alone. Therefore, in the *P Path* (Figure 1, orange box), we feed all retrieved events from the frozen  $R$  into  $P$  simultaneously, thereby training  $P$  to make predictions considering the correlation between events ((6)). During the evaluation, REMed relies solely on the *P Path*, drawing from the combined strengths of both  $R$  and  $P$ .

In this manner, we successfully built a powerful prediction model that can process a near-infinite unlimited number of events. By resolving the fundamental cause of the event selection, REMed significantly reduces the need for a domain expert’s involvement, ultimately resolving a significant bottleneck in the model-building process. For additional details, please refer to Appendix A.

#### 4. Cohorts and Experimental Settings

Even if REMed can bypass event selection, its practicality will be limited if this bypass decreases its prediction performance. While some research suggests that abstaining from

Table 1: Summary of tasks. For instance, there are two tailored tasks in the Length of Stay category: LOS-7day and LOS-14day. \*, \*\*, and \*\*\* represent binary, multi-class, and multi-label classification tasks, respectively. The additional detail can be found in Section B.

Category	Description
Mortality	Whether the patient will die within 1/2/3/7/14 days*.
Length of Stay (LOS)	Whether the length of ICU stay will be longer than 7/14 days*.
Readmission	Whether the patient will be readmitted to the ICU within the same hospital stay*.
Diagnosis	Predict all categories of diagnosis codes of the hospital admission**.
Creatinine	Predict the last creatinine measurement value occurred within 1/2/3 days after the prediction time***.
Platelets	Predict the last platelets measurement value occurred within 1/2/3 days after the prediction time***.
White Blood Cells	Predict the last WBC measurement value occurred within 1/2/3 days after the prediction time***.
Hemoglobin	Predict the last hemoglobin measurement value occurred within 1/2/3 days after the prediction time***.
Bicarbonate	Predict the last bicarbonate measurement value occurred within 1/2/3 days after the prediction time***.
Sodium	Predict the last sodium measurement value occurred within 1/2/3 days after the prediction time***.

feature selection does not compromise performance (Rajkomar et al., 2018; Nallabasannagari et al., 2020; Hur et al., 2022, 2023), there are no such results for observation window selection. Accordingly, we aim to demonstrate the following two key properties of REMed: 1) REMed can effectively handle long inputs compared to multiple baselines, and 2) the performance of REMed is not compromised when the observation window selection is bypassed. We validated these properties through extensive experiments using four publicly available EHR datasets: MIMIC-IV (Johnson et al., 2020), eICU (Pollard et al., 2018), UMCdb (Thorald et al., 2021), and HIRID (Hyland et al., 2020). These datasets are commonly employed in medical prediction research (McDermott et al., 2021; Hur et al., 2022, 2023), and their wide accessibility guarantees the reproducibility of our experiments by the research community. Furthermore, these datasets consist of EHRs from ICU-admitted patients, meaning the events are densely recorded (*i.e.*, a large number of medical events). This characteristic is advantageous for showcasing REMed’s strength in processing long inputs. We minimally filtered these datasets based on two criteria: patients who were adults (age > 18) and those with an ICU stay exceeding 48 hours. Detailed experimental setups can be found in Appendix B.

We demonstrated REMed’s robust capabilities under various conditions. First, we examined REMed and compared it with baselines using four datasets. Second, we tested our model at two prediction times: 24 hours and 48 hours after ICU admission. Third, we trained and evaluated our model on ten categories and 27 tailored medical prediction tasks (Table 1), in a multi-task manner<sup>4</sup>. In addition to the administrative prediction tasks commonly used in prior research (Rajkomar et al., 2018; Wang et al., 2020; McDermott et al., 2021; Steinberg et al., 2021; Hur et al., 2022, 2023), we further added frequent lab measurement prediction tasks that are closely related to a patient’s overall status.

<sup>4</sup>While examining REMed for each task can also showcase its robustness, building multiple models corresponding to each task comes with severe overhead in practical scenarios. Further discussion is provided in Appendix A.4.

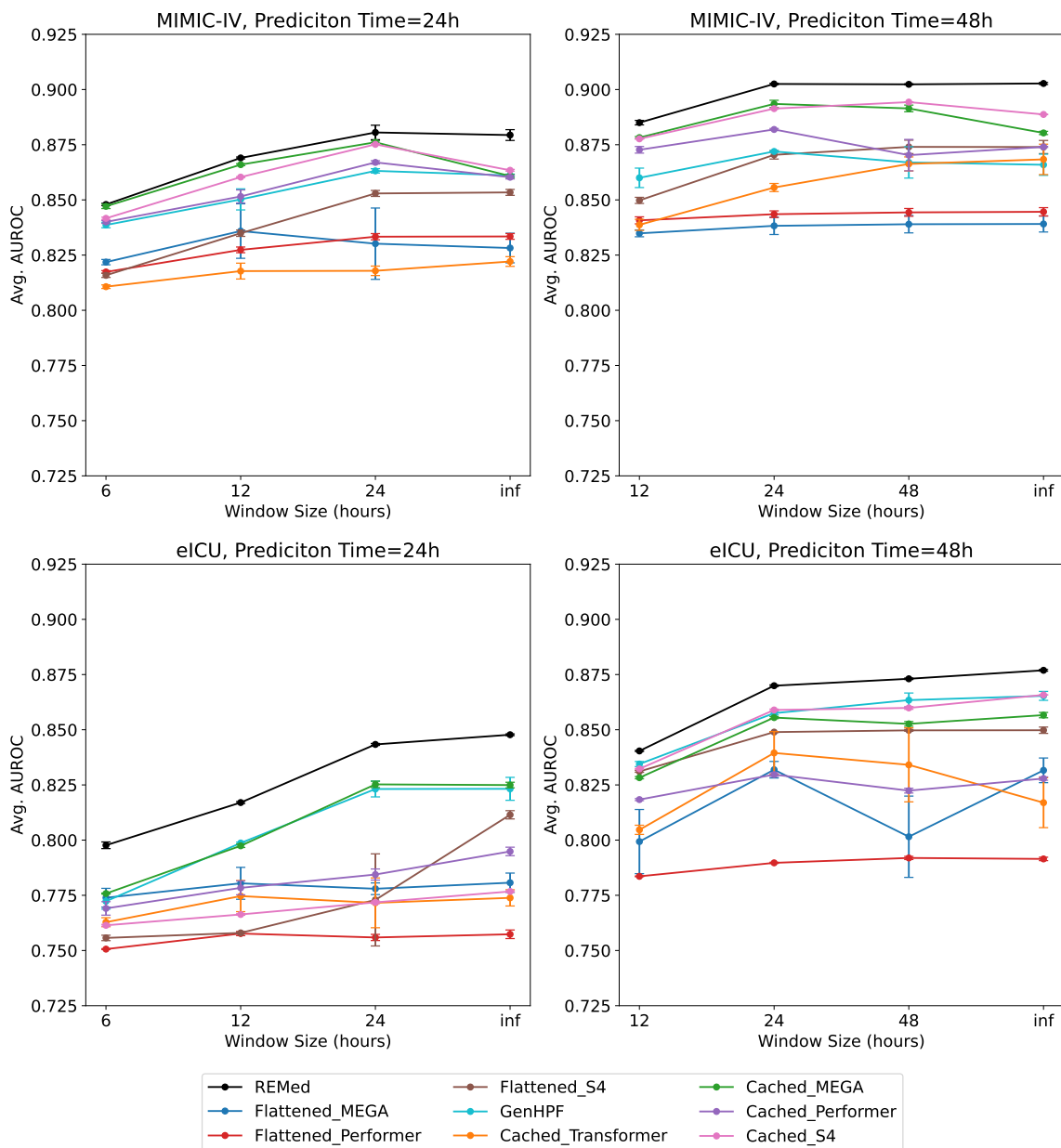


Figure 2: Performance Analysis Result on MIMIC-IV and eICU. We evaluated REMed and the baselines on two datasets, two prediction times, and multiple observation window sizes. The y-axis corresponds to the micro-average AUROC over tasks. The error bars represent the standard error of the mean for three runs with different random seeds.

We compared REMed with various baselines, including GenHPF (Hur et al., 2023) and its variants. *GenHPF*, the basis of our model, uses two Transformer (Vaswani et al., 2017) models in an end-to-end manner, one for encoding each medical event into a vector representation and another for making predictions. *Flattened* model, a variant proposed



in the same paper (Hur et al., 2023), concatenates all  $r_i$  in chronological order, and passes them to a single Transformer model. Additionally, we introduce *Cached* model, which uses the event vectors  $v_i$  as input to a single Transformer model, similar to REMed. Since all these baselines can only process a limited number of events, we prioritized the most recent events as input when the input size reaches the computational limit. Additionally, to partially alleviate this input size restriction, we replaced their backbone Transformer with modern, efficient architectures that are specialized for processing long inputs. Specifically, we selected Performer (Choromanski et al., 2020), S4 (Gu et al., 2021), and MEGA (Ma et al., 2022), which have demonstrated state-of-the-art performance in the benchmark for long input (Tay et al., 2020). This modification enables the baselines to handle a larger number of events. We also considered RMT (Bulatov et al., 2022) as a backbone; however, it failed to converge without the specific curriculum learning they proposed (Appendix C). Details about these baselines can be found in Appendix D.

## 5. Results

### 5.1. Performance Analysis

We primarily focus our experiments on MIMIC-IV and eICU, and further validate our findings using UMCdb and HIRID. The results are displayed in Figure 2. First, REMed outperformed all baseline models in most settings, regardless of whether the long or short observation window was used. To statistically affirm the superior prediction performance of REMed, we employed a one-sided Mann-Whitney U test (Mann and Whitney, 1947) on each dataset, prediction time, and observation window size, comparing it against the best baseline performance at each setting. The results substantiated REMed’s superiority in all settings ( $p < 0.05$ ), barring two cases (MIMIC-IV, prediction time 24h, observation windows 6h and 24h). Even for those two cases, our model’s performance was still on par with the best baselines. Therefore, we can conclude that REMed processes long input more effectively than the baselines.

We noticed a monotonic increase in our model’s prediction performance as the observation window length was extended. This is supported by the Kendall-Tau test (Kendall, 1938), with  $p$ -values ranging from 0.001 to 0.01 across all four graphs. Even though the performance plateaued in MIMIC-IV, no decrease was observed with longer windows. In contrast, the performance of most baseline models either plateaued or declined. Even for those that occasionally demonstrated monotonically increasing performance, their results were inconsistent across the four settings. We conclude that bypassing the observation window selection with REMed does not compromise the performance; the unlimited observation window consistently yields the best performance. We believe it is all the more valuable that REMed outperformed the baselines in the unlimited observation window scenarios.

To more rigorously demonstrate the two aforementioned properties, we expanded our experiments to include UMCdb and HIRID. To simplify the experiments, we focused on the 48-hour prediction window, which allows for longer input lengths. Furthermore, we excluded the flattened baselines, which consistently showed inferior performance in earlier experiments. The results of these experiments are illustrated in Figure 3. Following the same analytical approach as above, the Mann-Whitney U test validated the superiority of our model over the baselines with a significance level of  $p < 0.05$  in most cases. There

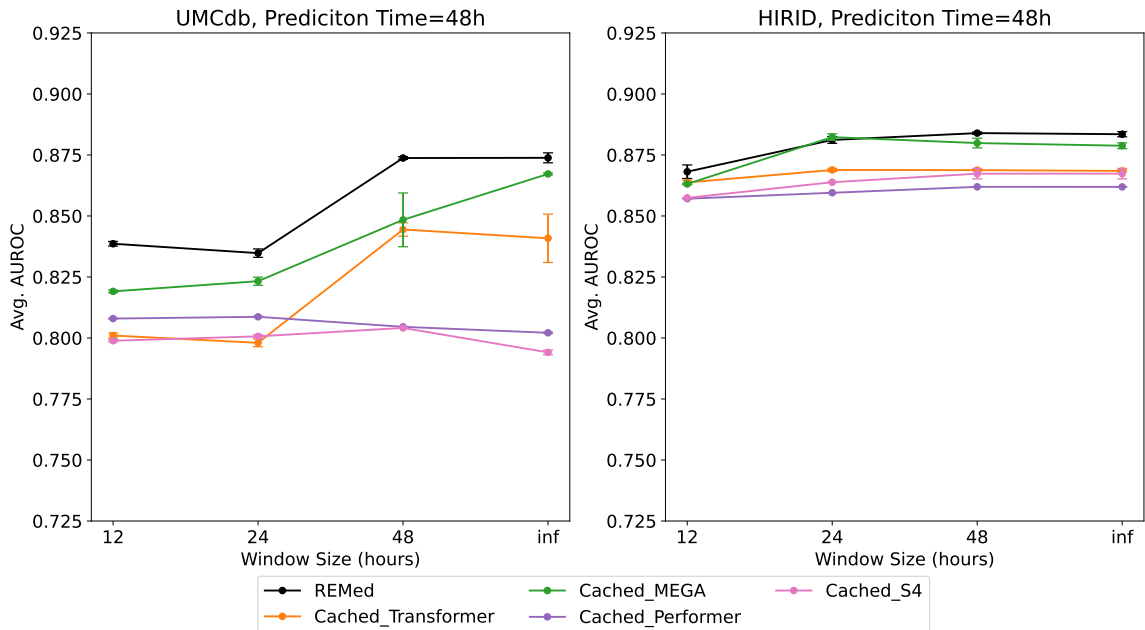


Figure 3: Performance Analysis Result on UMCdb and HIRID. We evaluated REMed and the baselines on multiple observation window sizes. The y-axis corresponds to the micro-average AUROC over tasks. The error bars represent the standard error of the mean for three runs with different random seeds.

were two exceptions for shorter window sizes in HIRID (12h and 24h); however, even in such cases, our model exhibited comparable performance to the best baseline. Similarly, the Kendall-Tau test verified that the prediction performance of our model monotonically increased as the observation window length increased for each dataset, with significance levels of  $p < 0.05$  and  $p < 0.01$ .

We conducted additional experiments to validate REMed’s robustness and strong performance. First, we analyzed the per-task performance from the previous experiments and confirmed that REMed consistently outperformed the baselines in most scenarios, demonstrating its task-wise generalizability (see Appendix E.1). Second, we repeated the previous experiment with a different model configuration and verified that the two aforementioned properties were maintained (see Appendix E.2). Lastly, we established that REMed provides a significant performance advantage over traditional regression models, despite its complexity (see Appendix E.3). Owing to this robust and powerful capability to process near-infinite events, REMed can minimize the need for manual involvement of domain experts, a common bottleneck in developing medical prediction models.

## 5.2. Retrieval Result Analysis

While retrieval-based models in the general domain measure their retrieval performance using labeled data, (Karpukhin et al., 2020; Lewis et al., 2020), there is no labeled data in medical prediction tasks (*i.e.*, ground-truth label indicating which event(s) must be

Table 2: The top-30 medical codes most frequently retrieved from MIMIC-IV (left) and eICU (right) are presented. ‘Avg. Ret.’ refers to the average number of times each code appears within the top  $k$  retrieved events when REMed makes a prediction. Codes in bold indicate that they are included in the union set of the top-30 codes selected by each clinician. The responses from each expert are displayed in Appendix F.

Table	Code	Avg. Ret
labevents	<b>Hemoglobin</b>	4.41
labevents	<b>Hematocrit</b>	3.61
chartevents	<b>Hematocrit (serum)</b>	3.46
labevents	<b>Bicarbonate</b>	2.8
labevents	<b>Platelet Count</b>	2.64
chartevents	<b>HCO<sub>3</sub> (serum)</b>	2.52
labevents	<b>Creatinine</b>	2.42
chartevents	<b>Respiratory Rate</b>	2.39
labevents	<b>White Blood Cells</b>	2.36
labevents	<b>Sodium</b>	2.35
chartevents	<b>WBC<sup>1</sup></b>	2.29
chartevents	<b>Heart Rhythm</b>	2.27
chartevents	Sodium (serum)	2.26
chartevents	<b>Creatinine (serum)</b>	2.15
labevents	<b>Calculated Total CO<sub>2</sub></b>	2.09
chartevents	<b>GCS<sup>2</sup>-Motor Response</b>	1.95
chartevents	Non Invasive BP <sup>3</sup> Diastolic	1.9
chartevents	<b>GCS<sup>2</sup>-Verbal Response</b>	1.73
chartevents	<b>Non Invasive BP<sup>3</sup>Systolic</b>	1.48
labevents	Chloride	1.46
chartevents	Chloride (serum)	1.45
labevents	MCHC <sup>4</sup>	1.33
labevents	Red Blood Cells	1.31
chartevents	Pulmonary Artery Pressure Mean	1.1
chartevents	<b>Mean Airway Pressure</b>	1.08
chartevents	O <sub>2</sub> Flow	1.05
chartevents	<b>Anion Gap</b>	0.99
chartevents	BUN <sup>5</sup>	0.99
outputevents	Foley	0.98
chartevents	<b>Non Invasive BP<sup>3</sup>Mean</b>	0.96

Table	Code	Avg. Ret
vitalPeriodic	<b>vitalPeriodic</b>	56.87
vitalAperiodic	<b>vitalAperiodic</b>	7.99
lab	<b>Hgb<sup>6</sup></b>	4.88
lab	<b>Hct<sup>7</sup></b>	4.58
lab	<b>Creatinine</b>	4.58
lab	<b>Platelets×1000</b>	3.59
lab	<b>WBC<sup>1</sup>×1000</b>	3.46
lab	<b>Sodium</b>	3.24
lab	RBC <sup>8</sup>	3.03
lab	<b>BUN<sup>5</sup></b>	2.53
lab	<b>Bicarbonate</b>	2.32
lab	Chloride	2.11
intakeOutput	Output (ml)   Urine	1.79
lab	<b>FiO<sub>2</sub><sup>9</sup></b>	1.27
lab	<b>paCO<sub>2</sub></b>	1.16
infusionDrug	Propofol (ml/hr)	1.09
lab	<b>O<sub>2</sub> Sat (%)</b>	1.00
nurseCharting	<b>Non-Invasive BP<sup>3</sup></b>	0.90
lab	<b>HCO<sub>3</sub></b>	0.82
lab	<b>Base Excess</b>	0.78
infusionDrug	Propofol (mcg/kg/min)	0.71
lab	<b>Lactate</b>	0.60
intakeOutput	Generic Intake (ml)   NS IVF <sup>10</sup>	0.59
lab	<b>paO<sub>2</sub></b>	0.56
lab	<b>pH</b>	0.50
lab	<b>Anion Gap</b>	0.48
infusionDrug	Fentanyl (mcg/hr)	0.48
lab	<b>Temperature</b>	0.45
infusionDrug	Fentanyl (ml/hr)	0.42
lab	PEEP <sup>11</sup>	0.38

<sup>1</sup> White Blood Cell<sup>2</sup> Glasgow Coma Scale<sup>3</sup> Blood Pressure<sup>4</sup> Mean Corpuscular Hemoglobin Concentration<sup>5</sup> Blood Urea Nitrogen<sup>6</sup> Hemoglobin<sup>7</sup> Hematocrit<sup>8</sup> Red Blood Cell<sup>9</sup> Fraction of Inspired Oxygen<sup>10</sup> Normal Saline Intravenous Fluid<sup>11</sup> Positive End-Expiratory Pressure

retrieved). Therefore, we indirectly measured the retrieval performance of the Retriever  $R$  by analyzing whether its behavior is compatible with established clinical knowledge. In this section, we exclusively focused on MIMIC-IV and eICU.

We first checked which medical codes  $c_i$  were frequently retrieved. We calculated the average number of events corresponding to a specific code retrieved every time the model makes a prediction for all test set samples. We narrowed our analysis to the 250 medical codes that occurred most frequently in the test set and used our best-performing models for each cohort. These best models were trained on a 48-hour prediction time and an unlimited observation window. Table 2 displays the top-30 most frequently retrieved codes from each cohort. Our model frequently retrieved codes related to core lab measurements, vital signs, neurologic status, analgesedative drugs, ventilation data, and input/output records.

To check whether these codes were truly useful for predicting the target tasks, we conducted an expert test involving two professors and a clinical fellow, all with expertise in the ICU. For each dataset, we showed them the same 250 codes and asked them to identify the 30 most significant ones. The average overlap of the top-30 codes between any two clinicians was 12.8 out of 30. While this overlap value might seem low, they do not necessarily indicate a lack of agreement. In fact, this reflects the complex nature of clinical decision-making, where multiple valid perspectives can exist. Clinicians may prioritize different codes based on their unique experiences and specialties, leading to a degree of variability in the selection. The degree of overlap between the top 30 codes of our model and each clinician’s selection averaged 10.9 out of 30. Although the agreement between the model and clinicians was slightly lower than that between two clinicians, this discrepancy may be due to inherent differences between models and human judgment. For instance, when both a high-level and low-level code (*e.g.*, a chart event code *heart rate alert* and a vital sign code *heart rate*) are available, clinicians tend to prefer the former, while REMed the latter. Given this, the alignment of our model’s choices with those of the clinicians was roughly equivalent to the alignment observed between different clinicians. This suggests that  $R$  can identify codes useful for the target task.

In addition to analyzing the medical code  $c_i$ , we explored the effects of the accompanied details  $d_i$  and the timestamp  $t_i$  on the behavior of the Retriever  $R$ .  $d_i$  is composed of various fields (*e.g.*, value, unit of measurement, flag, comment), and the composition varies based on the category of events, such as lab measurements or prescriptions, complicating the analysis. We specifically focused on lab measurement events associated with a platelets code, allowing us to clarify the fields of  $d_i$ . Typically,  $d_i$  for a lab measurement event includes “value”, “unit of measurement”, and “flag” fields. The “unit of measurement” remains consistent for the same code, and the “flag” is often derived from the “value”. Hence, we analyzed the scalar importance  $s_i$  in relation to  $t_i$  and the “value” for events associated with the lab codes used as prediction targets. Figure 4 (a) presents the results for the platelet measurement code, while the results for other codes are displayed in Appendix G.  $R$  assigned high scores to recent events or those with values in the abnormal range. These events are also regarded as important based on clinical knowledge. While peaks are observed around the ICU admission time, especially in the case of eICU, the lab results at this moment are typically regarded as pivotal in predicting future outcomes (Ferreira et al., 2001).

From the analysis presented above, the overall trends in both datasets are similar, but there are a few notable differences. These variations can be attributed to the unique

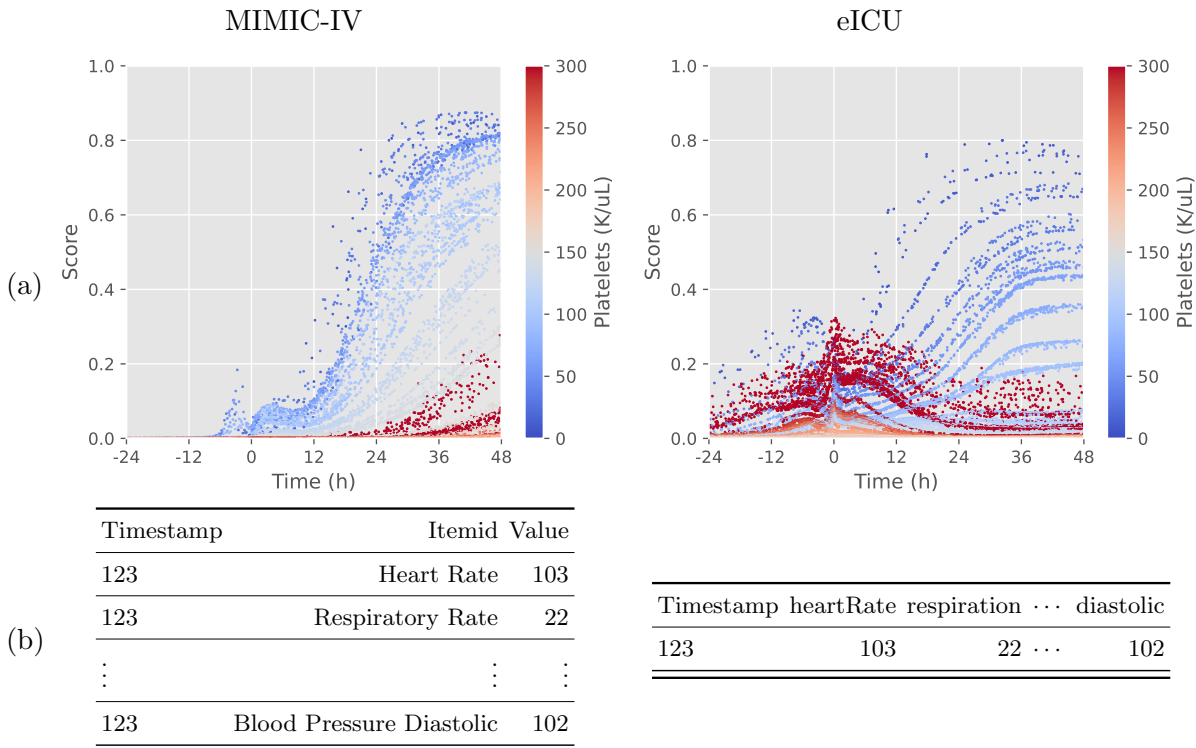


Figure 4: Retriever Analysis Result. The left column is for MIMIC-IV, and the right column is for eICU. (a) Allocated importance scores of platelets events against their timestamps and “value” fields. (b) Example of vital events from both datasets.

characteristics inherent in each dataset. For example, the “vitalPeriodic” code is frequently retrieved from eICU as seen in Table 2, whereas no single dominant code exists in MIMIC-IV. In the eICU EHR system, 16 types of vital signs—such as respiratory rate, heart rate, and blood pressure—are consolidated under a single event with the code “VitalPeriodic” (Figure 4 (b, right)). On the other hand, in MIMIC-IV, each vital sign is recorded as a separate event with its unique code (Figure 4 (b, left)). This leads to the frequent retrieval of events with the “vitalPeriodic” code in eICU, while in MIMIC-IV, events associated with various vital sign codes are retrieved more evenly. This behavior not only aligns with established clinical knowledge but also suggests REMed’s potential adaptability across different datasets.

In conclusion, the Retriever  $R$  can correctly identify useful events for predicting the target tasks, based on  $c_i$ ,  $d_i$ , and  $t_i$ , and its behavior was compatible with established clinical knowledge. Additionally, REMed showcased its adaptability to various characteristics of datasets.

## 6. Discussion

Utilizing structured EHR for medical prediction has been limited by the sheer volume of events, making the modeling process heavily reliant on expert opinions. By introducing a Retrieval-Based Approach (RBA) to medical prediction, we demonstrated that REMed

can process a near-infinite number of events, thereby reducing the need for domain expert involvement.

Besides, REMed also outperformed the baseline models in most settings. This superior performance can be analyzed by comparing it with the Cached Transformer since REMed’s Predictor uses a Transformer architecture. When input sizes exceed the Cached Transformer’s capacity, any performance gains can be attributed to the Retriever, which selects important past events that the Cached Transformer cannot observe. Conversely, when input sizes are shorter than the Cached Transformer’s capacity, the Cached Transformer can observe all events and is expected to perform equally well or better than REMed. However, REMed still outperforms it, indicating that the Retriever might help by filtering out noisy events and passing only the important ones to the Predictor, possibly acting as an additional regularizer. Further research is needed to clarify these observations.

We emphasize that our research solely relies on publicly available datasets and make our code publicly accessible for transparency and reproducibility. We believe that REMed can expedite the development of medical prediction models by reducing the dependency on domain experts.

### Limitations and Future Works

One of the major limitations of REMed is its inability to account for the correlation between events when evaluating the importance score  $s_i$ . Although the Predictor  $P$  can partially mitigate this limitation by considering the correlations in its predictions, this may not be sufficient for complex tasks where understanding the relationship between events is vital.

Another limitation of REMed is its need for retraining to adapt to new tasks, but there is room for improvement. Recently, the zero-shot (Wei et al., 2021) and few-shot (Brown et al., 2020) capabilities of large language models (LLMs) have been demonstrated for general domain tasks. This suggests that integrating LLMs with REMed might be able to lessen the burden of additional training for new tasks. However, smaller, supervised models often outperform LLMs on specific tasks since LLMs are primarily designed to predict the next natural language tokens autoregressively (Brown et al., 2020; Wei et al., 2021). Therefore, integrating medical prediction with LLMs remains a challenging task. Nevertheless, considering the rapid development of LLMs, it is worth exploring their potential for such applications.

While our framework primarily focuses on structured EHR data, it can be extendable to other modalities. For instance, since we use a pretrained text encoder to encode events, adapting our framework to handle unstructured EHRs (e.g., clinical notes) would be straightforward. Incorporating other modalities, such as chest X-ray images, would be more challenging as it would require additional modality-specific encoders, but it is feasible. Further work will be necessary to explore these potential extensions.

### Acknowledgments

This work was supported by the SNUBH-KAIST Joint Graduate Research Project on AI, the Institute of Information & Communications Technology Planning & Evaluation (IITP) grant (No.RS-2019-II190075), National Research Foundation of Korea (NRF) grant (NRF-2020H1D3A2A03100945), and Korea Medical Device Development Fund grant (Project

Number: 1711138160, KMDF\_PR\_20200901\_0097), funded by the Korea government (MSIT, MOTIE, MOHW, MFDS), Cloud TPUs from Google’s TPU Research Cloud (TRC).

## References

- Emily Alsentzer, John R Murphy, Willie Boag, Wei-Hung Weng, Di Jin, Tristan Naumann, WA Redmond, and Matthew BA McDermott. Publicly available clinical bert embeddings. NAACL HLT 2019, page 72, 2019.
- Sebastian Borgeaud, Arthur Mensch, Jordan Hoffmann, Trevor Cai, Eliza Rutherford, Katie Millican, George Bm Van Den Driessche, Jean-Baptiste Lespiau, Bogdan Damoc, Aidan Clark, et al. Improving language models by retrieving from trillions of tokens. In International conference on machine learning, pages 2206–2240. PMLR, 2022.
- Tom Brown, Benjamin Mann, Nick Ryder, Melanie Subbiah, Jared D Kaplan, Prafulla Dhariwal, Arvind Neelakantan, Pranav Shyam, Girish Sastry, Amanda Askell, et al. Language models are few-shot learners. Advances in neural information processing systems, 33:1877–1901, 2020.
- Aydar Bulatov, Yury Kuratov, and Mikhail Burtsev. Recurrent memory transformer. Advances in Neural Information Processing Systems, 35:11079–11091, 2022.
- Aydar Bulatov, Yuri Kuratov, and Mikhail S Burtsev. Scaling transformer to 1m tokens and beyond with rmt. arXiv preprint arXiv:2304.11062, 2023.
- Edward Choi, Mohammad Taha Bahadori, Jimeng Sun, Joshua Kulas, Andy Schuetz, and Walter Stewart. Retain: An interpretable predictive model for healthcare using reverse time attention mechanism. Advances in neural information processing systems, 29, 2016.
- Krzysztof Marcin Choromanski, Valerii Likhoshesterov, David Dohan, Xingyou Song, Andreea Gane, Tamas Sarlos, Peter Hawkins, Jared Quincy Davis, Afroz Mohiuddin, Lukasz Kaiser, et al. Rethinking attention with performers. In International Conference on Learning Representations, 2020.
- Jacob Deasy, Pietro Liò, and Ari Ercole. Dynamic survival prediction in intensive care units from heterogeneous time series without the need for variable selection or curation. Scientific Reports, 10(1):22129, 2020.
- Flavio Lopes Ferreira, Daliana Peres Bota, Annette Bross, Christian Mélot, and Jean-Louis Vincent. Serial evaluation of the sofa score to predict outcome in critically ill patients. Jama, 286(14):1754–1758, 2001.
- Albert Gu, Karan Goel, and Christopher Re. Efficiently modeling long sequences with structured state spaces. In International Conference on Learning Representations, 2021.
- Kyunghoon Hur, Jiyoung Lee, Jungwoo Oh, Wesley Price, Younghak Kim, and Edward Choi. Unifying heterogeneous electronic health records systems via text-based code embedding. In Conference on Health, Inference, and Learning, pages 183–203. PMLR, 2022.

- Kyunghoon Hur, Jungwoo Oh, Junu Kim, Jiyouon Kim, Min Jae Lee, Eunbyeol Cho, Seong-Eun Moon, Young-Hak Kim, Louis Atallah, and Edward Choi. Genhpf: General healthcare predictive framework for multi-task multi-source learning. IEEE Journal of Biomedical and Health Informatics, 2023.
- Stephanie L Hyland, Martin Faltys, Matthias Hüser, Xinrui Lyu, Thomas Gumbsch, Cristóbal Esteban, Christian Bock, Max Horn, Michael Moor, Bastian Rieck, et al. Early prediction of circulatory failure in the intensive care unit using machine learning. Nature medicine, 26(3):364–373, 2020.
- Sharon Jiang, Shannon Shen, Monica Agrawal, Barbara Lam, Nicholas Kurtzman, Steven Horng, David R Karger, and David Sontag. Conceptualizing machine learning for dynamic information retrieval of electronic health record notes. In Machine Learning for Healthcare Conference, pages 343–359. PMLR, 2023.
- Alistair Johnson, Lucas Bulgarelli, Tom Pollard, Steven Horng, Leo Anthony Celi, and Roger Mark. Mimic-iv. PhysioNet. Available online at: <https://physionet.org/content/mimiciv/1.0/>(accessed August 23, 2021), 2020.
- Alistair EW Johnson, Tom J Pollard, Lu Shen, Li-wei H Lehman, Mengling Feng, Mohammad Ghassemi, Benjamin Moody, Peter Szolovits, Leo Anthony Celi, and Roger G Mark. Mimic-iii, a freely accessible critical care database. Scientific data, 3(1):1–9, 2016.
- Vladimir Karpukhin, Barlas Oguz, Sewon Min, Patrick Lewis, Ledell Wu, Sergey Edunov, Danqi Chen, and Wen-tau Yih. Dense passage retrieval for open-domain question answering. In Proceedings of the 2020 Conference on Empirical Methods in Natural Language Processing (EMNLP), pages 6769–6781, 2020.
- Maurice G Kendall. A new measure of rank correlation. Biometrika, 30(1/2):81–93, 1938.
- Patrick Lewis, Ethan Perez, Aleksandra Piktus, Fabio Petroni, Vladimir Karpukhin, Naman Goyal, Heinrich Küttler, Mike Lewis, Wen-tau Yih, Tim Rocktäschel, et al. Retrieval-augmented generation for knowledge-intensive nlp tasks. Advances in Neural Information Processing Systems, 33:9459–9474, 2020.
- Xuezhe Ma, Chunting Zhou, Xiang Kong, Junxian He, Liangke Gui, Graham Neubig, Jonathan May, and Luke Zettlemoyer. Mega: Moving average equipped gated attention. In The Eleventh International Conference on Learning Representations, 2022.
- Henry B Mann and Donald R Whitney. On a test of whether one of two random variables is stochastically larger than the other. The annals of mathematical statistics, pages 50–60, 1947.
- Matthew McDermott, Bret Nestor, Evan Kim, Wancong Zhang, Anna Goldenberg, Peter Szolovits, and Marzyeh Ghassemi. A comprehensive ehr timeseries pre-training benchmark. In Proceedings of the Conference on Health, Inference, and Learning, pages 257–278, 2021.



- Aakanksha Naik, Sravanthi Parasa, Sergey Feldman, Lucy Lu Wang, and Tom Hope. Literature-augmented clinical outcome prediction. In Marine Carpuat, Marie-Catherine de Marneffe, and Ivan Vladimir Meza Ruiz, editors, Findings of the Association for Computational Linguistics: NAACL 2022, pages 438–453, Seattle, United States, July 2022. Association for Computational Linguistics. doi: 10.18653/v1/2022.findings-naacl.33. URL <https://aclanthology.org/2022.findings-naacl.33>.
- Anubhav Reddy Nallabasannagari, Madhu Reddiboina, Ryan Seltzer, Trevor Zeffiro, Ajay Sharma, and Mahendra Bhandari. All data inclusive, deep learning models to predict critical events in the medical information mart for intensive care iii database (mimic iii). arXiv preprint [arXiv:2009.01366](https://arxiv.org/abs/2009.01366), 2020.
- Tom J Pollard, Alistair EW Johnson, Jesse D Raffa, Leo A Celi, Roger G Mark, and Omar Badawi. The eicu collaborative research database, a freely available multi-center database for critical care research. Scientific data, 5(1):1–13, 2018.
- Alvin Rajkomar, Eyal Oren, Kai Chen, Andrew M Dai, Nissan Hajaj, Michaela Hardt, Peter J Liu, Xiaobing Liu, Jake Marcus, Mimi Sun, et al. Scalable and accurate deep learning with electronic health records. NPJ digital medicine, 1(1):18, 2018.
- Kirk Roberts, Matthew S. Simpson, Ellen M. Voorhees, and William R. Hersh. Overview of the trec 2015 clinical decision support track. In Ellen M. Voorhees and Angela Ellis, editors, TREC, volume 500-319 of NIST Special Publication. National Institute of Standards and Technology (NIST), 2015. URL <http://dblp.uni-trier.de/db/conf/trec/trec2015.html#RobertsSVH15>.
- Kirk Roberts, Dina Demner-Fushman, Ellen M. Voorhees, and William R. Hersh. Overview of the trec 2016 clinical decision support track. In Ellen M. Voorhees and Angela Ellis, editors, TREC, volume Special Publication 500-321. National Institute of Standards and Technology (NIST), 2016. URL <http://dblp.uni-trier.de/db/conf/trec/trec2016.html#RobertsDVH16>.
- David E Rumelhart, Geoffrey E Hinton, and Ronald J Williams. Learning internal representations by error propagation. Technical report, California Univ San Diego La Jolla Inst for Cognitive Science, 1985.
- L Nelson Sanchez-Pinto, Yuan Luo, and Matthew M Churpek. Big data and data science in critical care. Chest, 154(5):1239–1248, 2018.
- Matthew S Simpson, Ellen M Voorhees, and William R Hersh. Overview of the trec 2014 clinical decision support track. In TREC, 2014.
- Ethan Steinberg, Ken Jung, Jason A Fries, Conor K Corbin, Stephen R Pfohl, and Nigam H Shah. Language models are an effective representation learning technique for electronic health record data. Journal of biomedical informatics, 113:103637, 2021.
- Yi Tay, Mostafa Dehghani, Samira Abnar, Yikang Shen, Dara Bahri, Philip Pham, Jinfeng Rao, Liu Yang, Sebastian Ruder, and Donald Metzler. Long range arena: A benchmark for efficient transformers. In International Conference on Learning Representations, 2020.

- Patrick J Thorat, Jan M Peppink, Ronald H Driessen, Eric JG Sijbrands, Erwin JO Kompanje, Lewis Kaplan, Heatherlee Bailey, Jozef Kesecioglu, Maurizio Cecconi, Matthew Churpek, et al. Sharing icu patient data responsibly under the society of critical care medicine/european society of intensive care medicine joint data science collaboration: the amsterdam university medical centers database (amsterdamumcdb) example. Critical care medicine, 49(6):e563–e577, 2021.
- Ashish Vaswani, Noam Shazeer, Niki Parmar, Jakob Uszkoreit, Llion Jones, Aidan N Gomez, Lukasz Kaiser, and Illia Polosukhin. Attention is all you need. Advances in neural information processing systems, 30, 2017.
- Shirly Wang, Matthew BA McDermott, Geeticka Chauhan, Marzyeh Ghassemi, Michael C Hughes, and Tristan Naumann. Mimic-extract: A data extraction, preprocessing, and representation pipeline for mimic-iii. In Proceedings of the ACM conference on health, inference, and learning, pages 222–235, 2020.
- Jason Wei, Maarten Bosma, Vincent Zhao, Kelvin Guu, Adams Wei Yu, Brian Lester, Nan Du, Andrew M Dai, and Quoc V Le. Finetuned language models are zero-shot learners. In International Conference on Learning Representations, 2021.
- Xing Wei and Carsten Eickhoff. Embedding electronic health records for clinical information retrieval. arXiv preprint arXiv:1811.05402, 2018.
- Muchao Ye, Suhan Cui, Yaqing Wang, Junyu Luo, Cao Xiao, and Fenglong Ma. Medretriever: Target-driven interpretable health risk prediction via retrieving unstructured medical text. In Proceedings of the 30th ACM International Conference on Information & Knowledge Management, CIKM '21, page 2414–2423, New York, NY, USA, 2021. Association for Computing Machinery. ISBN 9781450384469. doi: 10.1145/3459637.3482273. URL <https://doi.org/10.1145/3459637.3482273>.

## Appendix A. Model Design

In this section, we describe the design choices of REMed. Unless specifically mentioned, all experiments described in this section are performed using the MIMIC-IV dataset, a 48-hour prediction time, and an unlimited observation window setting. All of the experiments were performed with a single A6000 48G GPU.

### A.1. Event Encoding

We investigated both unsupervised and supervised models for the event encoder  $Enc_{PT}$ , which encodes each event  $e_i$  into a vector  $v_i$ . First, we employed Bio-ClinicalBERT (Alsentzer et al., 2019), a derivative of BERT, further unsupervised pre-trained on biomedical and clinical domain literature. Despite its widespread use for clinical text encoding, it has been trained with MIMIC-III clinical notes, presenting two issues. 1) Since MIMIC-III and MIMIC-IV have overlapping patients, some of the samples in our test set might have been exposed during the training of the model. 2) There is a potential discrepancy in the distribution between note data and event data. To evaluate an unsupervised event encoder without these issues, we additionally trained a Transformer (Vaswani et al., 2017) from scratch with a masked language modeling objective. This model is trained using the text representations  $r_i$ 's as input, which originated from the training set of our MIMIC-IV cohort. Lastly, we used GenHPF (Hur et al., 2023), a supervised medical prediction model that employs two Transformers for event encoding and prediction. For our purposes, we trained GenHPF and employed the first Transformer as the event encoder.

We trained REMed using the  $v_i$ 's encoded by these models, respectively. From the preliminary evaluation, the version of REMed using  $v_i$ 's encoded with GenHPF achieved the best AUROC of 0.8747, compared to Bio-ClinicalBERT (0.7901) and MLM-based approach (0.8456).

However, GenHPF is primarily designed to predict based on a limited number of recent events. As a result, it struggles to encode events that occurred far back in a patient's history, such as emergency department events. To mitigate this, we randomly sampled events from the patient's entire history and fed them as input, thereby achieving an AUROC 0.9027 (top-right of Figure 2). We adopted this modified version of the GenHPF event encoder in all other experiments presented in this paper.

### A.2. Importance Scoring

In the Retrieval-Based Approach, both the question given by the user and documents are encoded as vectors. The cosine similarity between these vectors is then computed to determine the relevance of the documents to the question. To adapt this methodology for medical prediction, one might consider using a trainable vector that represents the predefined task (e.g., mortality prediction) and then measuring its cosine similarity with the event vectors. We preliminarily compared the cosine similarity method with the Multi-Layer Perceptron (MLP) method. For simplicity, we ignored  $t_i$  and used  $v_i$  exclusively as input in this comparison. The results indicated that the MLP method outperformed the cosine similarity method, with scores of 0.8898 versus 0.8849. Moreover, we encountered challenges when trying to incorporate temporal information, which can significantly affect the performance,

into the cosine similarity method. In contrast, when we concatenated  $v_i$  and  $t_i$  and input them into the MLP, there was a noticeable performance improvement, reaching an average AUROC of 0.9027. Using this scalar importance  $s_i$ , REMed retrieves the top- $k$  event vectors  $v_i$ . Empirical testing on the validation set, with  $k$  values ranging from 64 to 1024, revealed that setting  $k$  to 128 consistently delivered the best performance.

### A.3. Training Path

Using  $s_i$  to retrieve the top- $k$  documents cannot make the gradients reach the Retriever  $R$ . Hence,  $s_i$  must be directly involved in the final prediction to render  $R$  trainable. Furthermore,  $s_i$  must indicate the event’s importance to be used for top- $k$  retrieval. Incorporating  $s_i$  naively into equation 5 can satisfy the first requirement. This integration enables back-propagation from the prediction loss to  $R$ , allowing both  $R$  and  $P$  to be trainable end-to-end. However, because the top- $k$  retrieval operation does not propagate the gradient,  $P$  cannot recognize that  $s_j$  should reflect the importance of events, thus failing to meet the second requirement.

In contrast, our proposed method,  $R$  Path, effectively addresses both of these challenges. While  $s_i$  is directly involved in the final prediction,  $R$  is trained to increase  $s_i$  when  $\hat{y}_i$  is consistent with  $y$ . The  $s_i$  trained in this manner signifies the event’s importance, and can therefore be used for top- $k$  retrieval.

### A.4. Multi-Task Prediction

As previously mentioned, though training and evaluating medical prediction models for each prediction task is possible, this approach is impractical in real-world scenarios. The overhead involved in developing and operating numerous models makes using a single, multi-task model a more pragmatic choice. Thus, we evaluated our model in a multi-task setting to validate its robustness across various tasks and its practicality in real-world scenarios. For comparison, we also provide the model’s performance in a single-task setting. When we trained REMed for each task and averaged the AUROC, it yielded 0.8978. In contrast, the multi-task version of the model achieved 0.9027.

### A.5. Model Complexity and Near-Infinite History

REMed consists of an MLP Retriever  $R$  and a Transformer Predictor  $P$ .  $R$  evaluates each event vector independently, and each evaluation demands a constant amount of computation and memory. This means processing a patient’s history with  $R$  is linear in computational requirements relative to the number of events. On the other hand, although Transformer demands quadratic computational resources based on the input size (Vaswani et al., 2017),  $P$  always receives a fixed number of event vectors  $v_i$ , ensuring constant computational needs. Hence, REMed achieves linear complexity in computation and memory with the number of events, making it even more efficient than the contemporary architectures (Choromanski et al., 2020; Gu et al., 2021; Ma et al., 2022).

Under the finite observation windows, REMed’s memory consumption remained below 2GB. During the training of REMed with the longest hospital stay record, which consisted of 267k ( $\sim 2^{18}$ ) medical events corresponding to about 400 hospital days and 85 ICU days,

the peak memory usage was roughly 37GB. In evaluation mode, REMed processed up to  $2^{20}$  dummy events within the memory constraints of an A6000 48G GPU. Since this is four times longer than the extremest case among the four datasets, we claim that our model can process a near-infinite record of a single hospital admission.

## Appendix B. Experimental Detail

To maximize data utilization, we applied minimal filtering to our datasets: patients had to be over 18 years of age, and their ICU stays needed to exceed 48 hours. Additionally, we treated each ICU admission within a single hospital stay as a separate model input. For instance, under the 48-hour prediction time setting, if a patient was admitted to the ICU twice during a single hospital stay and each ICU stay exceeded 48 hours, we generated two separate model inputs. The first input spanned from the time of hospital admission to 48 hours after the first ICU admission. The second input spanned from the time of hospital admission to 48 hours after the second ICU admission, including the duration of the first ICU stay. We divided the cohorts into an 8:1:1 ratio for training, validation, and test sets. We also ensured that all ICU stays from a single patient were grouped into the same partition to prevent potential test set leakage. The statistics and label distribution for the datasets are provided in Tables 3-8.

For MIMIC-IV, we used the following tables: hosp/labevents, hosp/prescriptions, hosp/microbiologyevents, icu/inputevents, icu/chartevents, icu/outputevents, icu/procedureevents, ed/medrecon, ed/pyxis, ed/vitalsign, ed/diagnosis, and ed/triage. For eICU, we used the following tables: lab, medication, microLab, infusionDrug, intakeOutput, nurseCharting, nurseCare, nurseAssessment, treatment, vitalAperiodic, and vitalPeriodic. For UMCdb, we used the following tables: drugitems, freetextitems, listitems, numericitems, procedure-orderitems, processitems. For HIRID, we used the following tables: observation\_tables, pharma\_records. Note that events from the emergency department are only available in MIMIC-IV.

The UMCdb and HIRID offer more restricted information compared to MIMIC-IV and eICU, which affects the feasibility of certain tasks or necessitates adjustments. For instance, the lack of information in UMCdb for determining the order of ICU stays within a single hospital stay has led us to exclude the readmission task for this dataset. Moreover, while the diagnosis codes in MIMIC-IV and eICU were categorized according to the same system used in GenHPF (Hur et al., 2023), those in UMCdb do not align with this categorization, requiring a unique mapping approach. Regarding HIRID, it does not include ICU discharge times, crucial for filtering cohorts and defining some tasks. For cohort filtering, we considered patients with any event recorded more than 48 hours post ICU admission as having met the criteria. However, relying on this approximation for task labeling might introduce bias, prompting us to omit mortality and length of stay tasks. For reasons akin to those for UMCdb, we excluded the readmission task and applied a different categorization for diagnosis codes. The diagnosis code categorizations are displayed on Extended Table 4-6.

For both the baseline models and REMed, we conducted a grid search for the learning rate, ranging from  $1e-6$  to  $1e-3$ . We utilized a constant learning rate scheduler and included 500 warm-up steps. Early stopping was employed based on the validation AUROC, with patience set to 3 epochs. All experiments were performed using an A6000 48G GPU with

Table 3: Data Input Length Distribution

Dataset	Prediction Time (h)	Input Horizon (h)	# of Events				# of Tokens				
			average	median	90%	max	average	median	90%	max	
MIMIC-IV	24	6	344.9	327	539	1832	8002.9	7266	13149	48368	
		12	703.2	666	1056	3146	16534.0	15054	26381.4	83492	
		24	1601.2	1545	2279	5457	39454.1	36599	60227	148723	
		inf	2713.6	1748	3289.4	264838	67697.2	43441	90027.2	6621844	
	48	12	621.7	578	948	3198	13988.7	12539	22314	83327	
		24	1278.7	1188	1907	6409	29017.6	26035	45289.6	167210	
		48	2879.9	2772	4081	10928	68471.7	63959	101734.4	286674	
		inf	3992.4	3023	5106.2	266766	96714.8	72443	133924	6669451	
	eICU	24	6	175.7	153	293	1135	6766.3	5695	12358	43989
			12	360.3	315	593	2225	13931.8	11831	25173.3	83519
			24	774.8	687	1246	4825	30026.3	25898.5	53245	178635
			inf	1290.7	824	1838	140592	50954.9	32083	77627.6	5640899
48		12	329.7	293	544	4039	12532.3	10662	22923.3	166365	
		24	673.0	600	1096	4577	25715.8	22068	46326.2	187296	
		48	1447.8	1303	2318	8159	55742.1	48499.5	97743	304656	
		inf	1963.7	1464.5	3021	141509	76670.6	55958	126776.3	5673689	
UMCdb		48	12	6293.7	619	23887.6	57080	199068.8	31736	717089.8	1781734
			24	2816.2	1241	48189.2	113830	404977.9	63641	1456686.4	3552063
			48	26443.7	2559	95681.8	212686	835479.8	131369	2915309.2	6671146
			inf	26591.4	2698	96039.4	212766	842346.4	137966	2933463.6	6674956
HIRID	48	12	5315.1	5350	9212.2	15811	109802.0	108561	192767	321138	
		24	10941.5	11179	18422	31386	225919.5	226896	385757.8	632670	
		48	22328.0	22620	35702.2	60858	460126.2	461563	746492	1235864	
		inf	22332.8	22629	35703.8	60858	460233.6	461572	746519.2	1235864	

Table 4: MIMIC-IV and eICU Data Statistics and Diagnosis Label Distribution

Datasets		MIMIC-IV	eICU
Number of patients		25801	64276
Number of admissions		30360	72298
Number of icustays		32449	77718
Avg admission duration (d)		11.8	9.3
Avg ICU stay duration (d)		5.6	5.4
Avg. Age		64.1	64.3
Gender	Male	18280	42460
	Female	14169	35244
	Others/Unknown	-	7
Ethnicity	White	21981	59706
	Black	3318	9146
	Hispanic	1163	2866
	Asian	930	1290
	Others/Unknown	5057	3957
Diagnosis Label Distribution (Multilabel)			
Infectious and parasitic diseases		14848	13899
Neoplasms		10607	4979
Endocrine; nutritional; and metabolic diseases and immunity disorders		27826	22248
Diseases of the blood and blood-forming organs		19885	11958
Mental Illness		20370	10303
Diseases of the nervous system and sense organs		17189	14842
Diseases of the circulatory system		29491	45252
Diseases of the respiratory system		21338	35259
Diseases of the digestive system		20129	13803
Diseases of the genitourinary system		20411	21039
Complications of pregnancy; childbirth; and the puerperium		141	141
Diseases of the skin and subcutaneous tissue		4856	1617
Diseases of the musculoskeletal system and connective tissue		11483	1835
Congenital anomalies		1504	59
Injury and poisoning		16867	14150
Symptoms; signs; and ill-defined conditions and factors influencing health status		18741	13179
Residual codes; unclassified; all E codes [259. and 260.]		24490	6665

Table 5: UMCdb Data Statistics and Diagnosis Label Distribution

Datasets		UMCdb
Number of patients		7392
Number of admissions		-
Number of icustays		8359
Avg length of admissions (d)		-
Avg length of icustays		11.1187941141284
Avg. Age		-
Gender	Male	5223
	Female	2986
	Others/Unknown	-
Ethnicity	White	-
	Black	-
	Hispanic	-
	Asian	-
	Others/Unknown	-
Diagnosis Label Distrubution (Multilabel)		
Cardiovascular		1733
General Surgery		3083
Respiratory		856
Neurological		1096
Genitourinary/Renal		124
Gastrointestinal		444
Hematological		73
Transplant		18
Trauma		376
Metabolic		88
Musculoskeletal/Skin		56
Internal Medicine		2770
Non-Categorized/General		3491



Table 6: HIRID Data Statistics and Diagnosis Label Distribution

Datasets	HIRID	
Number of patients	-	
Number of admissions	-	
Number of icustays	9155	
Avg length of admissions (d)	-	
Avg length of icustays	-	
Avg. Age	62.2725286728563	
Gender	Male	5848
	Female	3307
	Others/Unknown	-
Ethnicity	White	-
	Black	-
	Hispanic	-
	Asian	-
	Others/Unknown	-
Diagnosis Label Distrubution (Multilabel)		
Cardiovascular	1893	
Pulmonary	1178	
Gastointestinal	1048	
Neurological	2410	
Sepsis + Intoxication	354	
Urogenital	24	
Trauma	806	
Metabolic/Endocrinology	198	
Hematology	51	
Other	186	
Surgical Cardiovascular	1010	
Surgical Respiratory	375	
Surgical Gastointestinal	256	
Surgical Neurological	896	
Surgical Trauma	264	
Surgical Urogenital	17	
Surgical Others	148	

Table 7: MIMIC-IV and eICU Label Distribution (binary/multiclass)

Datasets		MIMIC-IV							eICU					
Prediction Time (h)	Task	Prediction Window	0	1	2	3	4	NaN	0	1	2	3	4	NaN
24	Readmission	-	30360	2089	0	0	0	0	72298	5420	0	0	0	0
		7	25887	6562	0	0	0	0	62765	14953	0	0	0	0
		14	30374	2075	0	0	0	0	73508	4210	0	0	0	0
	Length of Stay	1	32296	153	0	0	0	0	77702	16	0	0	0	0
		2	31730	719	0	0	0	0	76452	1266	0	0	0	0
		3	31283	1166	0	0	0	0	75341	2377	0	0	0	0
	Mortality	7	30010	2439	0	0	0	0	72553	5165	0	0	0	0
		14	28935	3514	0	0	0	0	70414	7304	0	0	0	0
		1	18799	6234	2784	889	611	3132	41597	13775	6993	2389	2030	10934
	Creatinine	2	18461	5471	2297	800	496	4924	39847	11836	5903	2049	1768	16315
		3	17150	4895	1945	660	396	7403	34624	9760	4692	1685	1501	25456
		1	18751	7277	4054	1077	167	1123	41873	15053	8269	1929	362	10232
	Platelets	2	17927	6680	3889	1110	172	2671	37890	13862	7831	1968	415	15752
		3	17870	5204	2999	1012	174	5190	33430	10651	6228	1734	381	25294
		1	1191	20320	9805	0	0	1133	2182	42804	22931	0	0	9801
	WBC	2	1275	21064	7439	0	0	2671	2026	42260	18051	0	0	15381
		3	1335	20219	5722	0	0	5173	1794	37480	13476	0	0	24968
		1	4079	13071	9335	4838	0	1126	7945	25816	20906	14003	0	9048
	Hemoglobin	2	3956	13048	8620	4153	0	2672	7413	25365	18945	11316	0	14679
		3	3597	12223	7875	3560	0	5194	5852	22546	16088	8920	0	24312
		1	7933	18764	4788	0	0	964	15165	38746	12695	0	0	11112
	Bicarbonate	2	6069	17624	6307	0	0	2449	11439	35642	14353	0	0	16284
		3	4519	15809	7067	0	0	5054	7926	29860	14387	0	0	25545
		1	5986	22695	2855	0	0	913	11651	50147	8744	0	0	7176
Sodium	2	5313	21790	2967	0	0	2379	10415	45807	8964	0	0	12532	
	3	4297	20228	3114	0	0	4810	8458	38904	8236	0	0	22120	
	-	30360	2089	0	0	0	0	72298	5420	0	0	0	0	
48	Readmission	7	25887	6562	0	0	0	62765	14953	0	0	0	0	
		14	30374	2075	0	0	0	0	73508	4210	0	0	0	0
		1	31730	719	0	0	0	0	76452	1266	0	0	0	0
	Length of Stay	2	31283	1166	0	0	0	0	75341	2377	0	0	0	0
		3	30884	1565	0	0	0	0	74413	3305	0	0	0	0
		7	29803	2646	0	0	0	0	72116	5602	0	0	0	0
	Mortality	14	28834	3615	0	0	0	0	70249	7469	0	0	0	0
		1	18461	5471	2297	800	496	4924	39847	11836	5903	2049	1768	16315
		2	17150	4895	1945	660	396	7403	34624	9760	4692	1685	1501	25456
	Creatinine	3	15053	4268	1676	516	331	10605	29176	8113	3941	1386	1256	33846
		1	17927	6680	3889	1110	172	2671	33430	10651	6228	1734	381	25294
		2	17870	5204	2999	1012	174	5190	29359	7816	4714	1501	337	33991
	Platelets	3	16579	3843	2394	898	153	8582	2026	42260	18051	0	0	15381
		1	1275	21064	7439	0	0	2671	1794	37480	13476	0	0	24968
		2	1335	20219	5722	0	0	5173	1500	31226	11301	0	0	33691
	WBC	3	1218	17782	4895	0	0	8554	7413	25365	18945	11316	0	14679
		1	3956	13048	8620	4153	0	2672	5852	22546	16088	8920	0	24312
		2	3597	12223	7875	3560	0	5194	4840	19266	13302	7150	0	33160
	Hemoglobin	3	3215	10855	6795	3007	0	8577	11439	35642	14353	0	0	16284
		1	6069	17624	6307	0	0	2449	7926	29860	14387	0	0	25545
		2	4519	15809	7067	0	0	5054	5767	24342	13752	0	0	33857
	Bicarbonate	3	3528	13634	6878	0	0	8409	10415	45807	8964	0	0	12532
		1	5313	21790	2967	0	0	2379	8458	38904	8236	0	0	22120
		2	4297	20228	3114	0	0	4810	6936	32619	7337	0	0	30826
Sodium	3	3656	17709	2981	0	0	8103	8458	38904	8236	0	0	22120	

Table 8: UMCdb and HIRID Label Distribution (binary/multiclass)

Task	Datasets		UMCdb					HIRID						
	Prediction Window		0	1	2	3	4	NaN	0	1	2	3	4	NaN
Readmission	-	-	-	-	-	-	-	-	-	-	-	-	-	-
Length of Stay	7	4705	3654	0	0	0	0	-	-	-	-	-	-	-
	14	6411	1948	0	0	0	0	-	-	-	-	-	-	-
Mortality	1	8086	273	0	0	0	0	-	-	-	-	-	-	-
	2	7896	463	0	0	0	0	-	-	-	-	-	-	-
	3	7785	574	0	0	0	0	-	-	-	-	-	-	-
	7	7510	849	0	0	0	0	-	-	-	-	-	-	-
Creatinine	14	7251	1108	0	0	0	0	-	-	-	-	-	-	-
	1	4007	714	348	88	30	3172	4321	912	516	150	49	3207	
	2	3056	500	231	60	23	4489	2989	590	278	80	36	5182	
	3	2495	401	157	42	19	5245	2159	409	152	39	21	6375	
Platelets	1	4080	1679	1138	360	110	992	3647	1545	1310	426	141	2086	
	2	3368	1218	861	318	105	2489	2711	983	789	352	121	4199	
	3	3071	870	648	290	87	3393	2219	612	471	276	91	5486	
WBC	1	208	1108	3178	0	0	3865	254	4982	1925	0	0	1994	
	2	168	3333	2368	0	0	2490	176	3591	1252	0	0	4136	
	3	135	2889	1943	0	0	3392	134	2582	1026	0	0	5413	
Hemoglobin	1	418	3284	2791	1145	0	721	509	3622	2155	864	0	2005	
	2	313	2609	2255	847	0	2335	306	2654	1513	545	0	4137	
	3	272	2198	1903	713	0	3273	222	2005	1121	389	0	5418	
Bicarbonate	1	1661	4486	1271	0	0	941	823	4820	983	0	0	2529	
	2	921	3502	1461	0	0	2475	426	3285	882	0	0	4562	
	3	543	2880	1557	0	0	3379	303	2357	734	0	0	5761	

BF16 mixed precision, and each experiment was repeated using three different random seeds. Detailed hyperparameters for the models are provided in Table 9.

Table 9: Model Hyperparameters. For all of the models, we used batch size 8, 512 hidden dimensions. REMed is capable of processing a practically infinite number of events, even can handle the longest case in our dataset. Since both the REMed and the Cached models use a 2-layer pre-trained event encoder, we ensured that the total number of layers was matched.

Models		Max. Tokens	Max. Events	LR	No. of Layers (Trainable)	Model Size (M)
Flatten	Mega	8192	-	5e-4	4	28.1
	S4	16384	-	1e-4	4	28.9
	Performer	16384	-	5e-5	4	27.6
GenHPF	Transformer	-	512	5e-5	4	27.6
Cached	Transformer	-	4096	1e-5	2	6.4
	Mega	-	16384	5e-4	2	6.6
	S4	-	16384	1e-5	2	7.0
	Performer	-	32768	1e-5	2	6.4
REMed		-	$\infty$ (>267k)	1e-5	2	6.6

### Appendix C. Recurrent Memory Transformer

We also considered using the Recurrent Memory Transformer (RMT) (Bulatov et al., 2022), an architecture that can process virtually unlimited input with constant memory, as the backbone for our baselines. However, baselines with RMT did not converge unless we adopted a specific training method as the authors suggested (Bulatov et al., 2023). Using this method, which involves learning rate scheduling and curriculum learning, we compared REMed to baselines with RMT. We evaluated those on MIMIC-IV with a 48-hour prediction time setting, which has the longest average input sequence length in our studies.

The results are illustrated in Figure 5 (a). REMed’s performance remained relatively stable regardless of the training method used, and it consistently surpassed both the *Flattened* and *Cached* RMT (Mann-Whitney U test,  $p < 0.01$ ). Furthermore, as the observation window size expanded, REMed showed a monotonic performance increase, even with the addition of curriculum learning and scheduling (Kendall-Tau test,  $p < 0.01$ ), while the baseline performances often decreased.

### Appendix D. Baselines

*GenHPF* (Hur et al., 2023): This approach exploits the inherent hierarchies in EHR data. It employs two Transformers: the first one (*Enc*) encodes each  $r_i$  to a vector  $v_i$ , while the second one (*P*) aggregates these vectors for predictions.

$$\hat{y}_{GenHPF} = P(\{Enc(r_i), t_i\}) \quad (7)$$

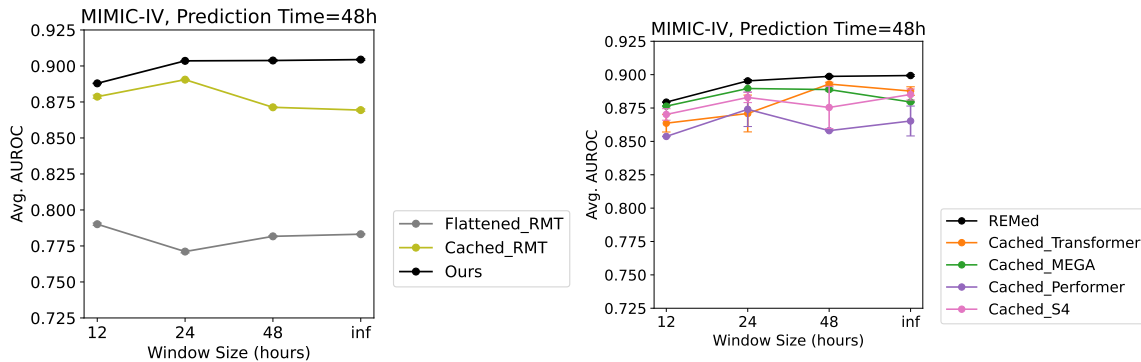


Figure 5: (a, left) Comparison with RMT. (b, right) Result for small model size ablation study. The error bars represent the standard error of the mean for three runs with different random seeds.

*Flattened* model (Hur et al., 2023): This approach chronologically concatenates all  $r_i$ ’s and then feeds them into a Transformer ( $P$ ) for predictions.

$$\hat{y}_{Flattened} = P(\text{Concat}(\{r_i\}), \{t_i\}) \quad (8)$$

*Cached* model: This approach utilizes  $v_i$ ’s encoded with the pre-trained text encoder  $Enc_{PT}$ , similar to that used in REMed. The predictor  $P$  receives these vectors as input and then makes a prediction. The absence of a trainable encoder reduces the computational demands, allowing the model to handle longer sequences.

$$v_i = Enc_{PT}(r_i), \hat{y}_{Cached} = P(\{v_i, t_i\}) \quad (9)$$

To make these models able to handle longer sequences, we used contemporary, efficient architectures (Choromanski et al., 2020; Gu et al., 2021; Ma et al., 2022) as their backbone (*i.e.*, replacing the vanilla Transformer). Theoretically, 12 baselines can be derived from these combinations, including the original Transformer version. However, not all combinations are practical. For *GenHPPF*, the computational bottleneck arises during the event encoding step. In this step, the encoder processes numerous  $r_i$ ’s independently, each consisting of several dozen tokens. Since the efficient architectures do not offer advantages for processing short inputs compared to Transformer, employing them for *GenHPPF* is not beneficial. As a result, we did not replace the Transformer backbone of *GenHPPF* with any contemporary architectures. On the other hand, for the *Flattened* model, using the Transformer backbone is impractical. The model’s strategy—to concatenate all  $r_i$ ’s—yields inputs with at least a few thousand tokens. Given the quadratic computational complexity of the Transformer, it’s infeasible to manage such long inputs using this backbone. Therefore, we only used contemporary architectures for the *Flattened* baseline. In summary, we constructed eight baselines: *GenHPPF*-Transformer, *Flattened*-Performer, S4, MEGA, *Cached*-Transformer, Performer, S4, and MEGA.

## Appendix E. Additional Performance Analysis

### E.1. Per-Task Performance Analysis

To assess the robustness of REMed across different prediction targets, we evaluated its performance on each task. We also focused on MIMIC-IV, 48-hour prediction time, and infinite input window scenario.

The results are displayed in Table 10. Overall, REMed outperformed all baselines in 23 of the 27 tasks, and its performance was comparable to the best baselines in the remaining four tasks. Based on these results, we conclude that REMed demonstrates strong generalizability across a diverse set of tasks.

### E.2. Model Size

In order to assess REMed’s robustness with respect to configuration, we expanded our experiment to another model size. For simplification, our analysis focused on the MIMIC-IV with a 48-hour prediction time, which has the longest average input length among our test scenarios. Furthermore, we only considered *Cached* baselines, previously shown to outperform others (*i.e.*, GenHPF and Flattened) in prior experiments. We configured REMed and the baselines with a hidden dimension of 128 and 4 heads, and conducted the same learning rate grid search for each model. The maximum sequence length for each baseline was adjusted to fit within a 12GB maximum memory allowance.

The results are presented in Figure 5 (b). Despite a reduced model size, REMed outperformed all baselines in every setting. The Mann-Whitney U test (Mann and Whitney, 1947) confirmed its superior performance over the best-performing baselines in each setting ( $p < 0.05$ ). Furthermore, the Kendall-Tau test (Kendall, 1938) verified a monotonic improvement in REMed’s performance by increasing the observation window length ( $p < 0.01$ ). These results suggest that REMed’s key properties hold across different configurations.

### E.3. Comparison to Regression Models

While machine learning models generally show superior performance compared to regression models, they require more resources for training and evaluation. To verify that REMed offers a significant performance benefit over regression models, justifying the complexity, we compared it with additional regression baselines. We focused on the MIMIC-IV dataset, with a 48-hour prediction time and an infinite input window scenario. We constructed logistic, Lasso, Ridge, and Lasso regression models with timestamps. The first three models use all unique codes as input features, while the model with timestamps uses bucketized codes categorized by timestamp as input: pre-ICU, 0-24 hours after ICU admission, and 24-48 hours after ICU admission.

As a result, the four models achieved average AUROC of 0.827, 0.841, 0.831, and 0.837, respectively. While these performances are comparable to the worst baselines under the same setting in Figure 2, these scores lag behind REMed’s performance (0.903). Given the need for precise predictions in the clinical domain, REMed’s advantages outweigh its complexity.

Table 10: Per-task performance analysis results: bold text indicates the best performance for each task.

AUROC	Mortality_1	Mortality_2	Mortality_3	Mortality_7	Mortality_14	LOS_7	LOS_14	Readmission	Diagnosis
Flatten_Mega	0.939	0.904	0.892	0.862	0.846	0.817	0.836	0.606	0.812
Flatten_Performer	0.947	0.911	0.894	0.874	0.861	0.817	0.835	0.572	0.829
Flatten_S4	<b>0.949</b>	0.920	0.899	0.882	0.864	0.820	0.840	0.585	0.831
GenHPF	0.935	0.896	0.885	0.860	0.845	0.807	0.828	0.608	0.830
Cached_Transformer	0.868	0.851	0.857	0.838	0.829	0.779	0.799	0.579	0.824
Cached_Mega	0.916	0.888	0.888	0.858	0.846	0.793	0.826	0.634	0.832
Cached_Performer	0.920	0.896	0.883	0.865	0.854	0.802	0.833	<b>0.647</b>	<b>0.844</b>
Cached_S4	0.943	0.921	<b>0.918</b>	0.870	0.856	0.823	0.848	0.617	0.832
REMed	0.939	<b>0.921</b>	0.907	<b>0.879</b>	<b>0.866</b>	<b>0.836</b>	<b>0.848</b>	0.606	0.832
AUROC	Creatinine_1	Creatinine_2	Creatinine_3	Platelets_1	Platelets_2	Platelets_3	WBC_1	WBC_2	WBC_3
Flatten_Mega	0.902	0.906	0.904	0.887	0.898	0.911	0.861	0.874	0.872
Flatten_Performer	0.910	0.915	0.913	0.896	0.909	0.918	0.867	0.883	0.881
Flatten_S4	0.961	0.957	0.951	0.941	0.939	0.941	0.887	0.896	0.892
GenHPF	0.962	0.954	0.949	0.924	0.927	0.934	0.881	0.894	0.890
Cached_Transformer	0.967	0.960	0.954	0.963	0.957	0.958	0.906	0.907	0.906
Cached_Mega	0.968	0.960	0.955	0.960	0.956	0.957	0.930	0.925	0.918
Cached_Performer	0.947	0.947	0.943	0.944	0.945	0.952	0.898	0.904	0.901
Cached_S4	0.969	0.964	0.958	0.952	0.954	0.957	0.924	0.918	0.910
REMed	<b>0.987</b>	<b>0.977</b>	<b>0.971</b>	<b>0.978</b>	<b>0.971</b>	<b>0.969</b>	<b>0.961</b>	<b>0.946</b>	<b>0.936</b>
AUROC	Hemoglobin_1	Hemoglobin_2	Hemoglobin_3	Bicarbonate_1	Bicarbonate_2	Bicarbonate_3	Sodium_1	Sodium_2	Sodium_3
Flatten_Mega	0.756	0.749	0.742	0.779	0.771	0.775	0.853	0.861	0.839
Flatten_Performer	0.758	0.755	0.750	0.779	0.778	0.777	0.862	0.869	0.846
Flatten_S4	0.854	0.831	0.816	0.848	0.832	0.813	0.890	0.888	0.868
GenHPF	0.831	0.809	0.795	0.846	0.828	0.815	0.895	0.888	0.865
Cached_Transformer	0.890	0.865	0.850	0.858	0.832	0.824	0.883	0.882	0.860
Cached_Mega	0.878	0.854	0.841	0.858	0.834	0.820	0.906	0.894	0.875
Cached_Performer	0.864	0.847	0.841	0.832	0.818	0.814	0.894	0.889	0.872
Cached_S4	0.893	0.865	0.849	0.872	0.848	0.835	0.915	0.903	0.882
REMed	<b>0.925</b>	<b>0.890</b>	<b>0.870</b>	<b>0.902</b>	<b>0.864</b>	<b>0.845</b>	<b>0.936</b>	<b>0.917</b>	<b>0.894</b>

## Appendix F. Extended Top-K Results

Table 11: MIMIC-IV Expert-Selected Top-30 Codes

<b>Annotator 1</b>	<b>Annotator 2</b>	<b>Annotator 3</b>
Skin Temperature	Heart Rate Alarm-Low	GCS-Verbal Response
Respiratory Pattern	fspn <sup>2</sup> High O <sub>2</sub> Saturation Pulseoxymetry Alarm-Low	
Breathing Pattern/Effort	Respiratory Pattern	Glucose
Norepinephrine	Breathing Pattern/Effort	Glucose (serum)
Respiratory Rate (total)	Norepinephrine	Respiratory Pattern
Arterial BP <sup>3</sup> Diastolic	Radial Pulse L	Norepinephrine
Inspired O <sub>2</sub> fraction	GCS <sup>1</sup> -Motor Response	GCS <sup>1</sup> -Motor Response
Respiratory Rate	Non-Invasive BP <sup>3</sup> Alarm-Low	GCS <sup>1</sup> Eye Opening
Peak Insp. Pressure	Arterial BP <sup>3</sup> Diastolic	White Blood Cells
Arterial BP <sup>3</sup> Mean	Inspired O <sub>2</sub> Fraction	Arterial BP <sup>3</sup> Diastolic
Impaired Tissue Perfusion NCP <sup>4</sup> Interventions	Creatinine (serum)	Creatinine (serum)
PTT <sup>5</sup>	Respiratory Rate	Respiratory Rate
Non Invasive BP <sup>3</sup> Mean	Arterial BP <sup>3</sup> Mean	Sodium
Altered Mental Status NCP <sup>4</sup> Interventions	Non Invasive BP <sup>3</sup> Systolic	Arterial BP <sup>3</sup> Mean
Mean Airway Pressure	Arterial BP <sup>3</sup> Systolic	Temperature Fahrenheit
Pupil Response Right	Non Invasive BP <sup>3</sup> Mean	Arterial BP <sup>3</sup> Systolic
Capillary Refill R	Respiratory Effort	Pupil Response Right
Capillary Refill L	Bicarbonate	Bicarbonate
Tidal Volume (observed)	Respiratory Rate (spontaneous)	Heart Rhythm
Pupil Size Right	Heart Rhythm	pH
Heart Rate	pH	Calculated Total CO <sub>2</sub>
HCO <sub>3</sub> (serum)	Potassium (serum)	Hemoglobin
Resp Alarm-High	Hemoglobin	Mental Status
spO <sub>2</sub> Desat Limit	Hematocrit (serum)	Platelet Count
pO <sub>2</sub>	Creatinine	WBC <sup>6</sup>
Heart Rate Alarm-High	pO <sub>2</sub>	Creatinine
Anion Gap	Heart Rate Alarm-High	HCO <sub>3</sub> (serum)
Level of Consciousness	Anion Gap	spO <sub>2</sub> Desat Limit
Pupil Response Left	Hematocrit	Level of Consciousness
Base Excess	Base Excess	Pupil Response Left

<sup>1</sup> Glasgow Coma Scale<sup>2</sup> Spontaneous Breathing Frequency<sup>3</sup> Blood Pressure<sup>4</sup> Nursing Care Plan<sup>5</sup> Partial Thromboplastin Time<sup>6</sup> White Blood Cell



Table 12: eICU Expert-Selected Top-30 Codes

<b>Annotator 1</b>	<b>Annotator 2</b>	<b>Annotator 3</b>
Heart Rate	PTT <sup>1</sup>	Heart Rate
SV <sup>2</sup>	Lactate	Lactate
Norepinephrine (mcg/min)	PT <sup>3</sup>	Invasive BP <sup>4</sup>
Non-Invasive BP <sup>4</sup>	Norepinephrine (mcg/min)	Pupils Right
spO <sub>2</sub>	Invasive BP <sup>4</sup>	Vent Rate
Pupils Right	spO <sub>2</sub>	Platelets x1000
O <sub>2</sub> Saturation	Base Deficit	HCO <sub>3</sub>
Bicarbonate	Respiratory Assessment	Bicarbonate
O <sub>2</sub> Sat (%)	vitalPeriodic	Pupils Left
Pupils Left	O <sub>2</sub> Saturation	Glasgow Coma Score
Glasgow Coma Score	HCO <sub>3</sub>	Norepinephrine (mcg/kg/min)
paO <sub>2</sub>	Total CO <sub>2</sub>	Pupils
Mechanical Ventilation	Bicarbonate	pH
Symptoms of Delirium Present	O <sub>2</sub> Sat (%)	Vasopressin (units/min)
Temperature	Glasgow Coma Score	Respiratory Rate
Score (Glasgow Coma Scale)	paO <sub>2</sub>	Vasopressin (ml/hr)
O <sub>2</sub> Content	Hct <sup>5</sup>	Phenylephrine (ml/hr)
Respiratory Rate	pH	Norepinephrine (ml/hr)
Vasopressin (ml/hr)	Respiratory Rate	WBC x1000
PT <sup>3</sup> -INR <sup>6</sup>	Vasopressin (ml/hr)	fiO <sub>2</sub> <sup>7</sup>
Norepinephrine (ml/hr)	vitalAperiodic	MAP <sup>8</sup> (mmhg)
MAP <sup>8</sup> (mmhg)	Norepinephrine (ml/hr)	Pulse
Capillary Refill	MAP <sup>8</sup> (mmhg)	BUN <sup>9</sup>
paCO <sub>2</sub>	paCO <sub>2</sub>	Hgb <sup>10</sup>
Pulse	Hgb <sup>10</sup>	Mental Status Assessment
Mental Status Assessment	BNP <sup>11</sup>	Sodium
Crystalloids	Anion Gap	Anion Gap
Anion Gap	Arterial Line MAP <sup>8</sup> (mmhg)	Phenylephrine (mcg/min)
Arterial Line MAP <sup>8</sup> (mmhg)	Base Excess	Arterial Line MAP <sup>8</sup> (mmhg)
Base Excess	Creatinine	Creatinine

<sup>1</sup> Partial Thromboplastin Time

<sup>2</sup> Stroke Volume

<sup>3</sup> Prothrombin Time

<sup>4</sup> Blood Pressure

<sup>5</sup> Hematocrit

<sup>6</sup> International Normalized Ratio

<sup>7</sup> Fraction of Inspired Oxygen

<sup>8</sup> Mean Arterial Pressure

<sup>9</sup> Blood Urea Nitrogen

<sup>10</sup> Hemoglobin

<sup>11</sup> B-type natriuretic peptide

### Appendix G. Extended Importance Score Analysis

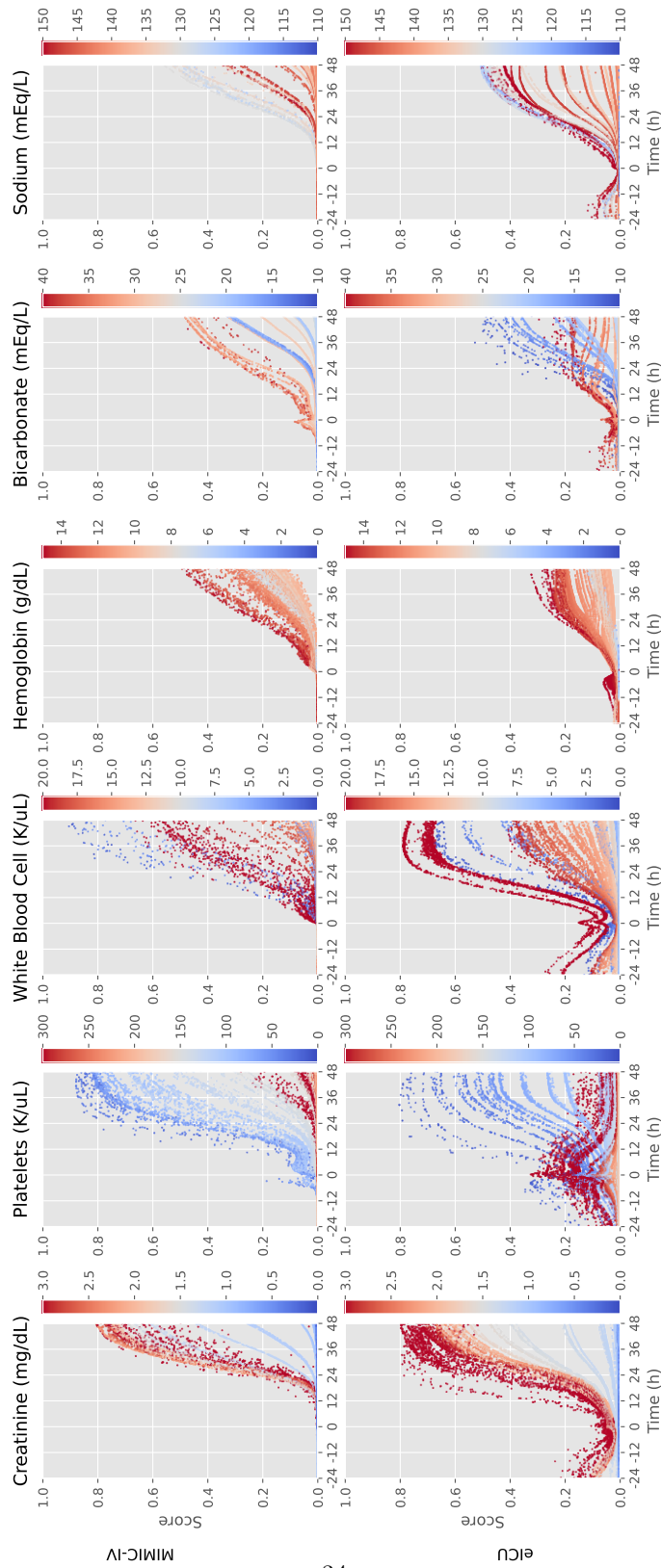


Figure 6: Extended Importance Score Analysis Results